JSR Publications

Available Online

J. Sci. Res. **15** (3), 667-684 (2023)

JOURNAL OF SCIENTIFIC RESEARCH

www.banglajol.info/index.php/JSR

Green Synthesis of Cobalt Oxide Nanoparticles (Co_3O_4 NPs) using *Bauhinia Racemosa* (Thiruvachi) Leaves Extract and Its antioxidant, anti-diabetic, and Anti-inflammatory Properties

G. Vanitha[1], R. Manikandan [1,2], A. Prakasam[1,3], M. D. Navinkumar[1,4], K. Sathiyamoorthi[5], B. Dhinakaran[1*]

[1]PG and Research Department of Physics, Government Arts College, Chidambaram, Tamilnadu, India-608001

[2]Munna College of Education, Parangipettai, Tamil Nadu, India-608502

[3]PG and Research Department of Physics, Aringar Anna Arts College, Villupuram, Tamilnadu, India-605602

[4]Vivekanadan College of Education, Puducherry, India-605008

[5]PG and Research Department of Chemistry, Government Arts College, Chidambaram, Tamilnadu, India-608001

Received 14 January 2023, accepted in final revised form 29 May 2023

Abstract

This study aims to appraise the antioxidant, anti-diabetic, and anti-inflammatory accomplishments of green synthesized cobalt oxide nanoparticles (Co_3O_4 NPs) mediated by *Bauhinia racemosa* leaves. *Bauhinia racemosa is commonly called "Thiruvachi' leaf tree in Tamil*. The green synthesized Co_3O_4 NPs are calcinated at 350 °C, then characterized by TG/DTA, UV, FTIR, FL, XRD, DLS, SEM with EDS analysis, TEM, and Supercapacitor performance studies with CV analysis. TGA/DTA result associated with weight loss and exothermic reaction due to desorption of chemisorbed water. FTIR was performed to identify the functional groups of carbonyl, hydroxyl, amine, and protein molecules, which form a layer covering Co_3O_4 NPs and stabilize the Co_3O_4 NPs in the medium. The XRD pattern peaks are associated with a poly cubic crystalline form of metallic cobalt oxide nanoparticles. The average grain size of Co_3O_4 NPs is 36.45 nm. This research focused on Biological studies like antioxidant, anti-diabetic, and anti-inflammatory, total antioxidant measured by phosphomolyptenium reagent with vitamin C as the standard, Anti-diabetics studies carried out by α-amylase inhibition method and anti-inflammatory bustle followed by BSA denaturation technique. The spectral and morphological data confirms the Co_3O_4 NPs formation. The anti-inflammatory activity showed good results than the antioxidant and anti-diabetic activity.

Keywords: Green synthesis; *Bauhinia racemosa*; Co_3O_4 NPs; Characterization; CV studies; Antioxidant; Anti-diabetics; Anti-inflammatory activity.

doi: http://doi.org/10.3329/jsr.v15i3.63884 J. Sci. Res. **15** (3), 667-684 (2023)

1. Introduction

The metal and metal oxide nanoparticles (NPs) possess unique characteristic features such as catalytic activity, thermal conductivity, optical, mechanical, and electronic properties,

* *Corresponding author*: drbdphysics@gmail.com

and biological activity owing to the higher outward zone-to-volume ratio, specific composition, shape, and size [1–3]. These unique properties make them highly useful in diverse filed like water pollution remediation, electrical, medicinal, self-cleaning, electrochemical sensing, and agricultural technology [4–7]. To make metal nanoparticles (MNPs), numerous ways with chemical wet processing, thermal reduction, micro-emulsion techniques, and biosynthesis approach using microorganisms (bacteria and fungi) and extracts of natural plants have been reported in the literature [8–11]. Among these various methods, plant-mediated (using extract of natural plants) creation of metal NPs (MNPs) is highly advantageous in terms of biocompatibility, non-toxic reagents, low energy requirement, rapid synthesis, ease of processing, easy scale-up and sustainable stability of synthesized nanoparticles as related to the wet chemical processing or physical itineraries of production [12]. The necessity of surfactant and steadying proxies through nanoparticle synthesis can be dodged by reworking the plant extract-used green synthesis approach. The chief phytochemical components (flavonoids, alkaloids, steroids, sulfhydryl terpenoids, sugars, and their derivatives molecules) with hydroxyl, allyl, amino, carboxylic, and alkoxy groups present in the plant extracts are not only beneficial as a reducing mediator in the synthesis of metallic NPs but also act as a steadying agent to maintain the long-term reactivity of NPs. Co_3O_4 NPs are archetypal d-block metal oxide and own magnetic p-type semiconductors and fascinating catalytic possessions [13,14]. Cobaltous oxide (CoO), cobaltic oxide (Co_2O_3), and cobaltosic oxide (Co_3O_4) are the major categories of cobalt-based NPs in various oxidation states [15]. Among these, Co_3O_4 NPs were widely employed in various applications, including energy storage and remediation of water pollution from groundwater and wastewater since the surface effects and variable oxidation state of cobalt (one-third with þ2 and two-third with þ3 oxidation state) [16]. They also act as catalysts of viable prominence and oxidative dehydrogenation, hydrogenation, and hydrogenolysis of the esters (R-COOR) group [17]. And yet cobalt metal NPs (Co NPs) have admirable possessions; their worse surface area and loftier crystalline size affected their practical utilization at large scale in real applications. It has been reported that physiognomies of the prepared nanoparticles depend on the type and part of the plants utilized for synthesis because of variations in the constituents and composition of phytochemicals in the extracts. In the recent past, a substantial amount of research studies have been steered using plant-mediated green synthesis methodology on the improvements of cobalt oxide nanoparticles properties. Therefore, in this article, recent advancements of cobalt nanoparticle synthesis through green routs using extracts of *Bauhinia racemosa* leaves (Fig. 1). The synthesized Co_3O_4 NPs are characterized, and pharmacological studies such as anti-inflammatory, antioxidant, and anti-diabetics activities.

Fig. 1. *Bauhinia racemosa* healthy leaves.

2. Material and Methods

2.1. *Collection of sample*

Fresh *Bauhinia racemosa healthy leaves* (Thiruvachi) leaves were collected from the botanical garden, Department of Botany, Government arts college, Chidambaram. Leaves were washed thoroughly three times by running ordinary tap water (OTW), then twice with double distilled water (DDW) to remove any dust particles on the leaves; washed leaves were allowed to dry in air at room temperature. The dried leaves were grained and powdered by using an electric mixer. This powder was used to prepare the leaves extracts.

2.2. *Chemicals, solvents, and starting materials*

De-ionized water, Whatman 1≠ and Whatman 41≠ filter papers, cobalt nitrate hexahydrate ($Co(NO_3)_2$. $6H_2O$, sodium hydroxide pellets, hydrochloric acids, and other chemicals were purchased from Merck (India) Ltd. All chemicals were used without further purification.

2.3. *Instruments and equipment*

Electric oven, Magnetic stirrer (REMI 2 MLH), E-1 portable TDS & EC meter,pH-009(I)A pen type pH meter, sterilized 250ml separating funnels, sterilized conical flasks, sterilized 400ml beakers, watch glasses, 7" funnels, glass rods, and 10ml measuring cylinders.

2.4. *Plant material processing*

5 g of *Bauhinia racemosa healthy* (Thiruvachi) leaves powder with 50 mL of double-distilled water (DDW) taken in the 250 mL round-bottomed flask; the water condenser

was fitted and fixed the running tap water then heated for 20 min at 80 °C. Then the extract was filtered with Whatman 1≠ filter paper. The filtrate was used to further the green synthesis of the process.

2.5. *Biosynthesis procedure*

For the synthesis of Cobalt oxide nanoparticles by reducing cobalt nitrate hexahydrate (M.F: $Co(NO_3)_2.6H_2O$, MW: 291.04 g/mol), 180 mL of a homogenous solution of cobalt nitrate is steadily mixed with 10 mL of leaves extract followed by continuous heating (70 °C) and stirring at 500 rpm for 3 h at magnetic stirrer with the heating instrument, to achieve reddish pink solution [18], The obtained brownish red color solution was added with 0.1 M NaOH solution maintain by pH 10, the solution was changed to blue color precipitate. The obtained precipitate was filtered with Whatman 1# filter paper. The precipitate was dried and powdered, then calcinated at 350 ^oC through a muffle furnace, after calcination to obtain gray color fine crystalline Co_3O_4 NPs. Finally, Co_3O_4 NPs were steadily characterized. Fig. 2 shows the scheme of green synthesis of cobalt oxide nanoparticles.

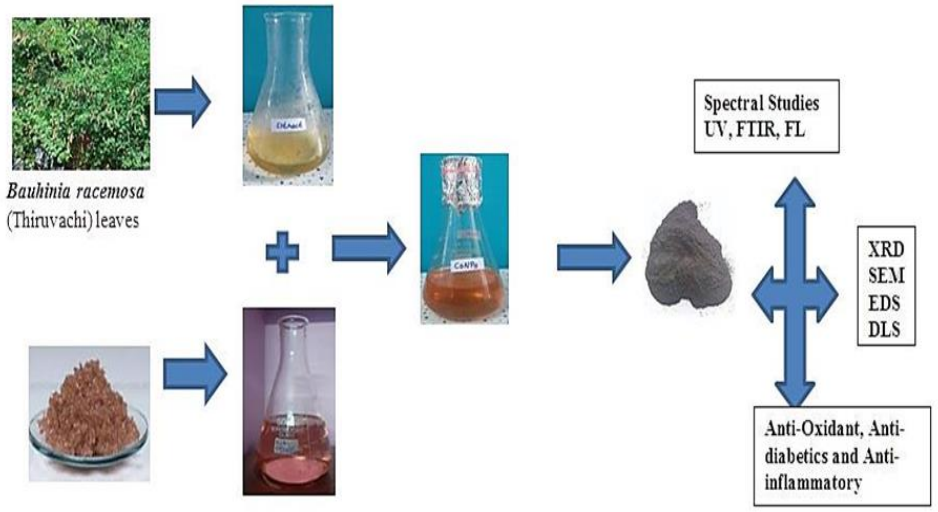

Fig. 2. Scheme of green synthesis of Co_3O_4 NPs mediated by *Bauhinia Racemosa.*

2.6. *Characterization*

The thermal stability of the powder sample determined by TG/DTA analysis was performed using NETZSCH-STA 449 F3 JUPITER; the Morphology, shapes, and nature of the nanoparticles were studied via SEM using image J software. The morphological identification was carried out through SEM, and Energy Dispersive X-ray spectroscopy (EDS) was also carried out. From the Department of Physics CISL, Annamalai

University, Annamalai Nagar, Tamil Nadu. Another morphology and shape with determining the size of the cobalt oxide particles using VIT Vellore's (High-Resolution Transmission Electron Microscope. The selected electron diffraction patterns (SEAD) areas were recorded by dispersing the sample onto a carbon-covered copper grid. The UV–Vis spectra were chronicled at laboratory temperature using a k-Helios SP Pye-Unicam spectrophotometer. FTIR spectra were recorded at room temperature on a Nicolet 6700 FTIR spectrometer. For the FTIR capacities of enclosed Co_3O_4 NPs, a lesser amount of Co_3O_4 NPs (0.01 g) dried at 60 °C for 4 h was assorted with KBr to form a pellet-like round disk suitable for FTIR measurements. To obtain the FTIR spectrum of the extract, an appropriate amount of the extract was mixed with KBr. Fluorescence spectra were recorded at room temperature on Perkin Elmer (LS 45) Range: 200 to 900 nm. In fluorescence spectrometry, both an excitation spectrum (the light that is absorbed by the sample) and/or an emission spectrum (the light emitted by the sample) can be measured; Electrical studies were approved out at room temperature on Princeton Applied Research (Versa STAT MC) Frequency: 1 Hz to 1 MHz. Cyclic Voltammetry (CV) is an electrochemical technique that trials the current that progresses in an electrochemical cell under circumstances where voltage is in extra of that prophesied by the Nernst equation. CV is achieved by cycling the potential of a working electrode and assessing the occasioning current from the ACIC instrumentation center at St. Joseph College, Trichy-02. X-ray diffraction (XRD) pattern was obtained by reducing a diffractometer with Shimadzu XRD-6000, Cu Ka (k= 1.54056 Å) to confirm the green synthesis of cobalt oxide nanoparticles from International Research Centre**,** Kalasalingam University, Krishnankoil, Virudhunagar, Also cobalt oxide nanoparticles performed by anti-inflammatory, antioxidant and anti-diabetic activities.

3. Result and Discussion

3.1. *TG/DTA analysis*

Synchronized thermo gravimetric and differential thermal analyses (TG/DTA) of the cobalt oxide nanoparticles with *Bauhinia racemosa* (Thiruvachi) are performed in the temperature range from 38 ºC to 1000 ºC at the rate of 20 ºC/min. TG/DTA study [19] of the as-prepared product is shown in Fig. 3. It has measured three predictable weight losses from the TG curve. The first weight losses are observed in the range of 100 ºC to 250 ºC (3 %) due to the desorption of water molecules. The second weight loss of (21 %) has been observed in the range of 250 ºC to 320 ºC owing to the decomposition of nitrate and other organic templates. The third weight loss of (8 %) was observed in the range of 320 to 380 ºC due to the phase transitions of the sample. No weight losses are predicted beyond 685 ºC, confirming the formation of Co_3O_4 NPs. The DTA curve shows a small endothermic peak at 250 ºC due to water molecules' desorption. The endothermic peak observed in the range of 380 ºC is due to the decomposition of nitrates in the synthesized sample.

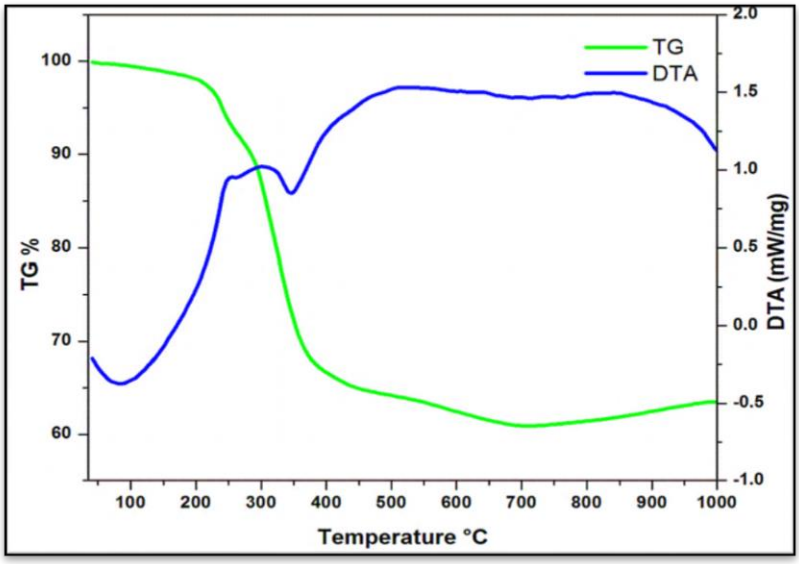

Fig. 3. TG/DTA Analysis of Co_3O_4 NPs by *Bauhinia racemosa* (Thiruvachi).

3.2. *Spectral and morphological studies*

3.2.1. *UV spectral analysis*

The UV-vis spectra of Co_3O_4 NPs mediated by *Bauhinia racemosa* (Thiruvachi) leaves colloids obtained by using ethanol solvent. Fig. 4 shows the UV spectrum; the surface Plasmon resonance band is wide, representing poly-dispersed nanoparticles. A flat and thin absorption band at 395 nm is observed, characteristic of mono-dispersed spherical nanoparticles. UV-visible spectroscopy is one of the most widely used techniques for structural characterization of Co_3O_4 NPs. The surface Plasmon resonance (SPR) band (λ max) around 395 nm broadened and slightly moved to the long wavelength region, indicating the presence and formation of Co_3O_4 NPs. The optical absorption spectra of metal nanoparticles are dominated by surface plasmon resonances, which change to lengthier wavelengths with increasing particle size. The position and shape of the plasmon absorption of cobalt nano-clusters are strappingly reliant on the particle size, dielectric medium, and surface-adsorbed species. The surface plasmon absorption of Co_3O_4 NPs has a short wavelength band in the visible region nearby 395 nm owing to the crosswise electric swinging.

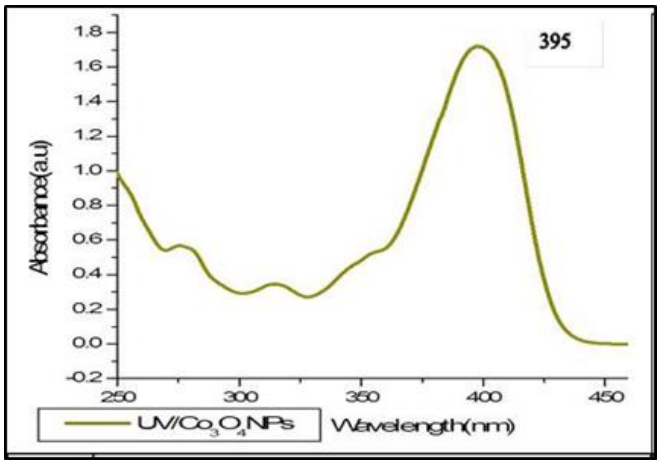

Fig. 4. UV Spectrum of Co_3O_4 NPs by *Bauhinia racemosa* (Thiruvachi).

3.2.2. *FTIR spectral analysis*

FTIR studies are very applicable to identifying phytoconstituents of the green materials; Gawade *et al.* [20] reported that ethanol extract of *Bauhinia racemosa* contained alkaloids, carbohydrates, protein and amino acids, glycoside, tannin, saponin, flavonoids, steroids, tri-terpenoids, and phenolic compounds. FTIR analysis was approved to categorize the conceivable biomolecules responsible for efficient stabilization, and capping agent of Co NPs synthesized using *Bauhinia racemosa* (Thiruvachi) leaves aqueous extract. Fig. 5a shows the FTIR spectrum for crude leaves powder of *Bauhinia racemosa* (Thiruvachi), Fig. 5b shows the FTIR spectrum for aqueous leaves extract of *Bauhinia racemosa* (Thiruvachi), and Fig. 5c shows the FTIR spectrum for Co_3O_4 NPs prepared by *Bauhinia racemosa* (Thiruvachi) leaves aqueous extract. In the IR spectrum of *Bauhinia racemosa* (Thiruvachi) leaves crude powder contain many phytochemical compounds, this spectrum have shown in usual far-reaching peak and very low percentage of transmittance at 3450 cm^{-1} indicates the –OH hydrogen bonds, The peak of 2924 and 2853 cm^{-1} has shown in –C-H overlapping with –OH bonding, The sharp peaks of 1645 cm^{-1} indicates –CO stretching vibration for saturated and unsaturated ketones, the sharp medium peaks appears at doublet formation of 1452 and 1384 cm^{-1} has indicates deformation of -CH_2- and -CH_3 bending vibrations, the broad peak at 1069 cm^{-1} stretching vibration of carboxylic acid and derivatives of carboxylic acids contain O-C group, the small sharp peaks at 848 and 781 cm^{-1} have indicates -COOR adsorption peaks, The peaks of 603 cm^{-1} have indicates alkyl halides peaks of –C-X bending vibrations. In the FTIR spectrum of aqueous extract of *Bauhinia racemosa* (Thiruvachi) leaves have shown in Fig. 5b the sharp peak of 3416 cm^{-1} have indicates –OH stretching vibration, 2924 cm^{-1} have indicates overlapping of –C-H in –OH bonding The sharp doublet peaks at 1635 cm^{-1} have reveals that the carbonyl stretching vibrations. The peaks of 1249 cm^{-1} stretching vibration of –CN bonding and the sharp peaks of 1073 cm^{-1} have shown C-C-C bending

vibration. The FTIR spectrum of Co_3O_4 NPs by *Bauhinia racemosa* (Thiruvachi) leaves aqueous extract have shown in Fig. 5c. 3425 cm^{-1} with decreased transmittance because cobalt metal ions reduce the various –OH group-containing group to alcohols, 2925 cm^{-1} have merged with –OH, C-H stretching and N-H bonding. The 1631 and 1106 cm^{-1} peaks have evidence of CO stretching and C-C-C bending vibrations.

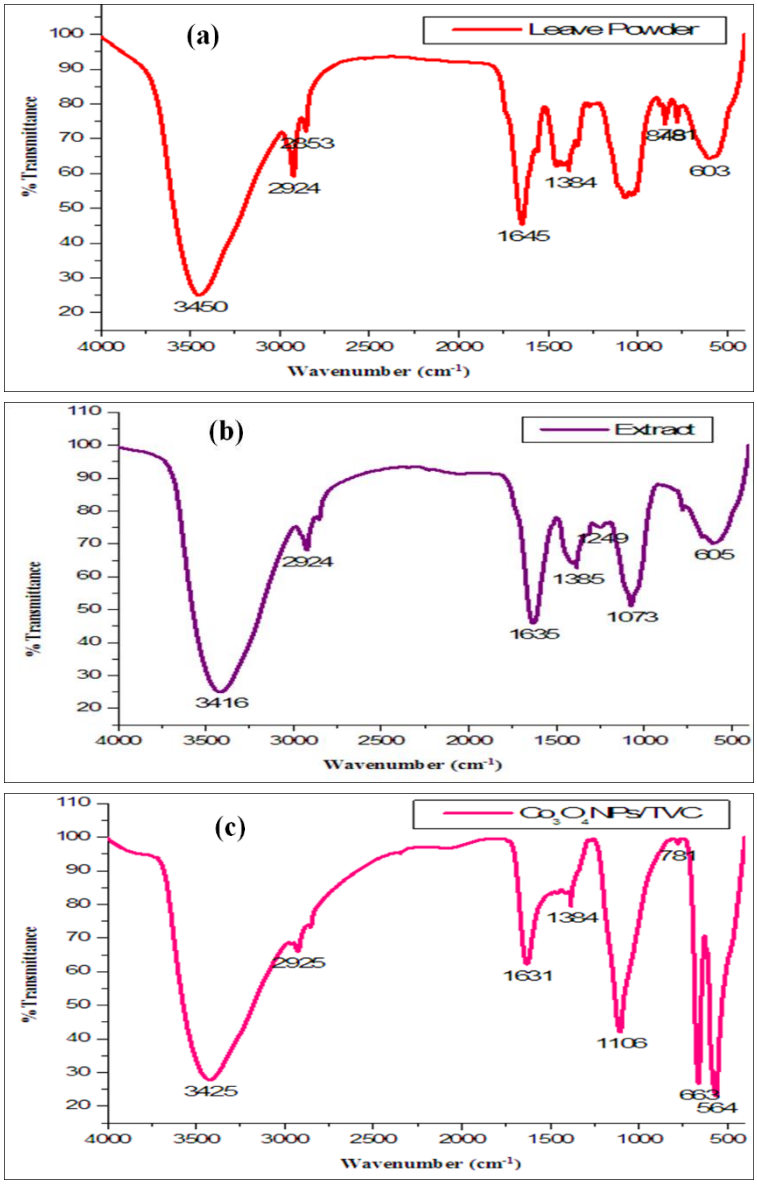

Fig. 5. (a) FTIR spectra of *Bauhinia racemosa* crude leaf powder, (b) aqueous extract of *Bauhinia racemosa* leaf and (c) Co_3O_4 NPs.

The IR spectrum of Co_3O_4 exhibits two major bands at 663 and 564 cm^{-1}. The first band is associated with the Co^{3+} vibration in the octahedral hole, and the second band (ν) is attributed to the Co^{2+} vibration in the tetrahedral hole, which confirms the formation of the Co_3O_4 spinel. The above three FTIR spectra revealed that the leave powder spectrum has more phytoconstituents, the Aqueous extract spectrum has shown only the water-soluble phytoconstituents, and finally, Co_3O_4 NPs FTIR shows the reduced peaks of cobalt ions (Co^{3+} and Co^{2+}) ions reduced the various phytoconstituents.

3.2.3. *Fluorescence spectroscopy analysis*

The spectral characteristics of fluorophores must match the wavelengths of the excitation light, Dichroic, and emission filters of the fluorescence microscope on which the experiments are to be done. Moreover, it is advised that their spectra are well separated from the spectra of other fluorophores that will be used simultaneously in the experiments to minimize cross-talk and bleed-through, which can give rise to [21] false co-localization and misinterpretations if not appropriately corrected. For use with advanced optical techniques (such as higher solution microscopies, two-photon microscopy, fluorescence lifetime imaging, spectral imaging, or correlation spectroscopy), further photo-physical aspects (e.g., lifetime, blinking, and environmental sensitivity) must also be taken into account. Fig. 6a shows the fluorescence emission of Co_3O_4 NPs; It shows that the plasmonic resonance is in the range close to 515 nm.

3.2.4. *XRD analysis*

XRD of Co_3O_4 NPs was synthesized from *Bauhinia racemosa* (Thiruvachi) aqueous leaf extract. The Co_3O_4 NPs were polycrystalline by description (JCPDS Card no. 042-1467) and phase structure, cubic shape, used as search technique with the ensemble as that efficacious chemical picas are divergent and no trace of humidity dust concentrations are engorged, as were apt for the sample. The average crystallite size of the Co_3O_4 NPs was calculated using the Debye-Scherrer equation):

$$D = K \lambda/\beta \cos\theta \quad (1)$$

Where: D is the particle size (in nm), k is a constant equal to 0.94, λ is the wavelength of X-Ray radiation (1.541A), β is the full-width at half maximum (FWHM) of the peak (in radians), and 2 theta is the Bragg angle (in degrees). The average crystallite size was found to be in the range of (21-55 nm). This belongs to the Co element present, making the nanoparticles smaller (4.9 nm). Depending on the XRD analysis, Okwunodulu *et al*. refer to the synthesis of Co_3O_4 NPs with 25-40 nm by *Magifera indica Leaf Extract* [22]. Malathy *et al*. refer to the synthesis of Co_3O_4 NPs with 50 nm by *Cadiospermum halicacebium* leaves extract [23]. This difference in size belongs to differences in reducing agents (plant extracts). A number of Bragg values are Co_3O_4 NPs by *Bauhinia racemosa* (Thiruvachi) leaves (111, 220, 311, 222, 400, 422, 511, 531) XRD pattern indicates that the Co_3O_4 NPs (Fig. 6b).

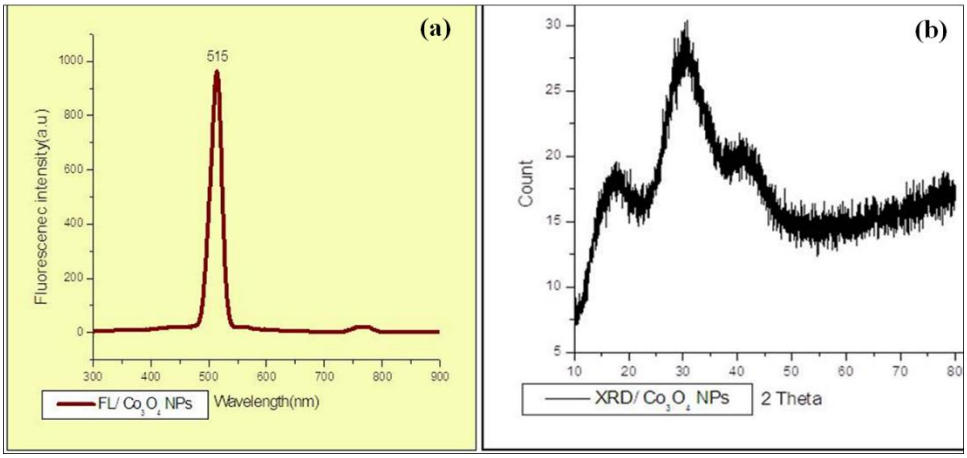

Fig. 6. (a) FL spectrum of Co_3O_4 NPs, (b) XRD spectrum of Co_3O_4 NPs *by Bauhinia racemosa* leaf extract.

3.2.5. *SEM analysis*

The surface morphology of the nanoparticles was determined by analyzing the structure by SEM. SEM images in Figs. 7(a-d) shows irregular rocky, cubic, hexagonal, and spherical shapes of various agglomerated sizes. Further observations with higher magnifications reveal that these images possess smooth surfaces. Biomolecules from leaf extract act as stabilizing and capping agent, which forms a coating on the discrete nanoparticles and holds hydroxyl group, which causes intermolecular hydrogen bonding ensuing in agglomeration [24]. This agglomeration is contingent upon the nature and mixes present in the extract; eco-toxic properties of transition metal oxide are due to the shape, small size, high chemical reactivity, biological activity, and agglomeration tendency, which causes threats to the environment and human beings.

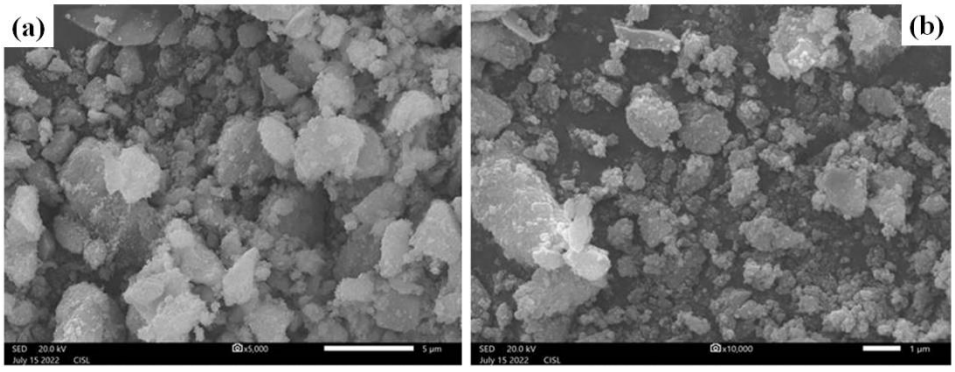

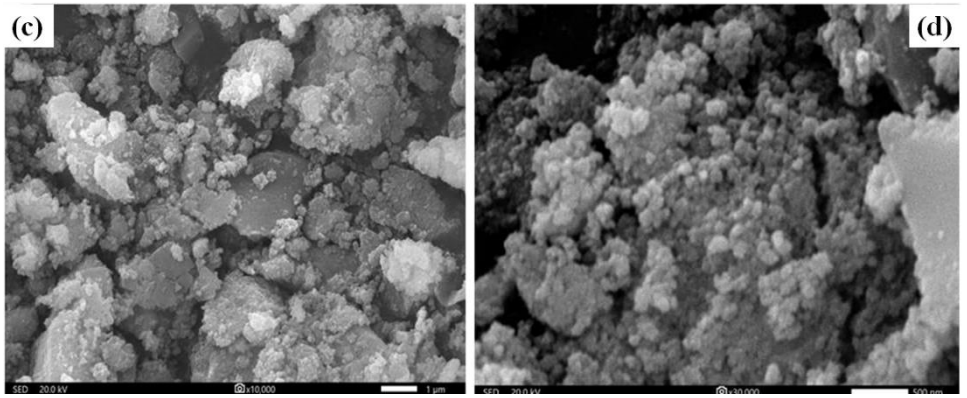

Fig.7. SEM images of Co_3O_4 NPs *by Bauhinia racemosa* leaf extract.

3.2.6. *EDS analysis*

The obtained results show strong signals at 0.8, 5.1, 6.8, and 7.8 keV were for Co and intense signals between 0.0-0.5 keV for oxygen portentous that Co and O were the major elements and construction of synthesis of cobalt oxide ascend from the sample and further unpredicted weak signals at 0.3, 1.9, 2.1, 2.7, 3.1, and 9.8 keV were from bio-compounds present in the leaf extract. The investigation of the EDS image and EDS spectrum is also shown in Figs. 8(a-b), the composition atom percentage (%) of oxygen is 49.86±0.26 %, the mass percentage of oxygen is 21.26±0.11 and the atom percentage of cobalt is 50.14±0.22 %. The mass percentage of cobalt is 78.74±0.35; other impurities are slightly presented. The trace amounts of cobalt demonstrated that plant phytochemical groups are involved in reducing and capping synthesized Co_3O_4 NPs.

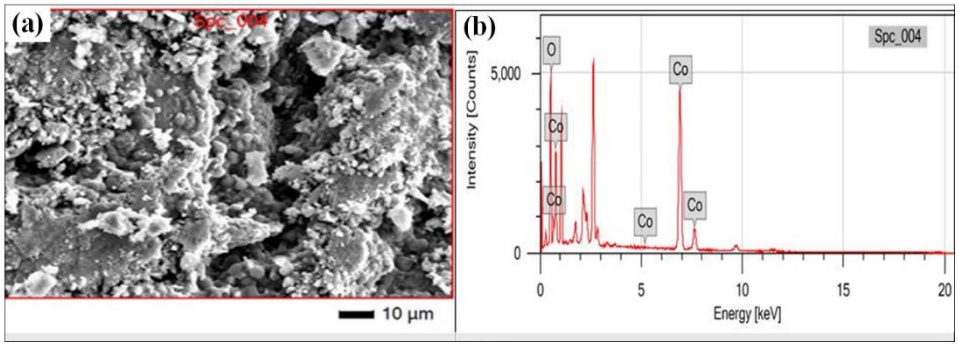

Fig. 8. (a) EDS image of Co_3O_4 NPs, (b) EDS spectrum of Co_3O_4 NPs.

3.2.7 TEM Analysis

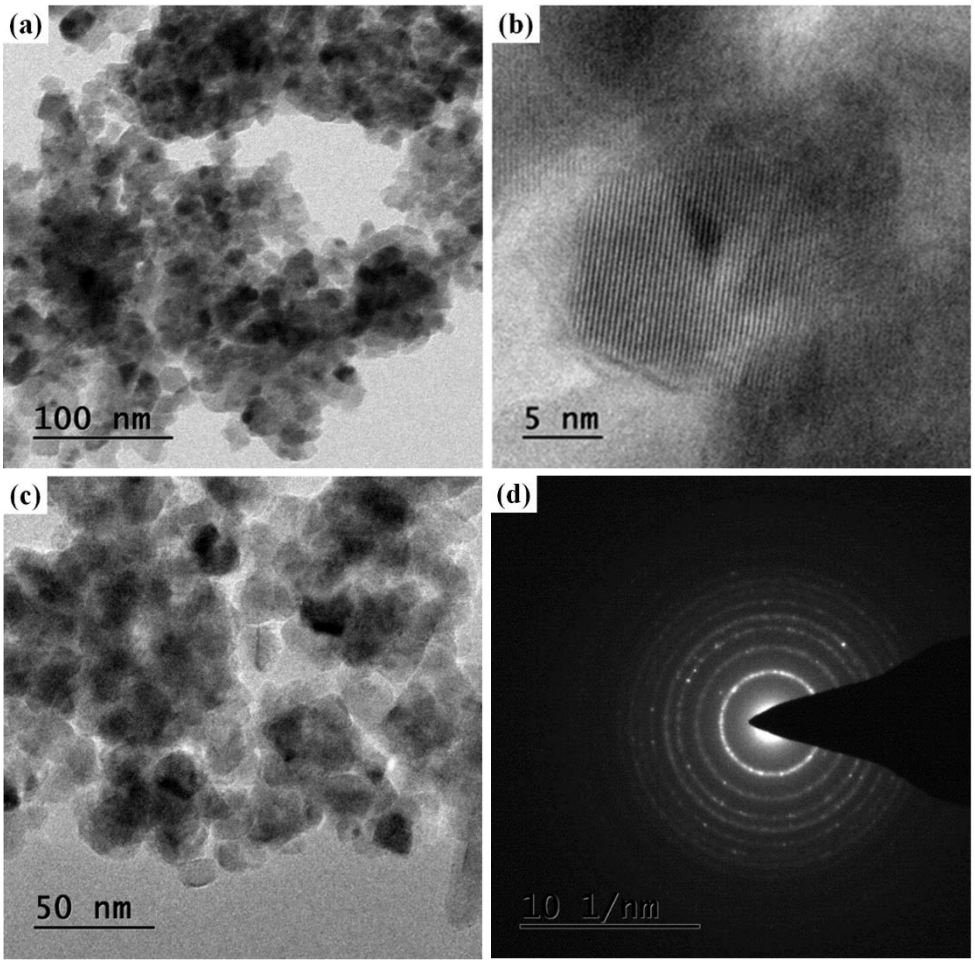

Fig. 9. TEM images of Co_3O_4 NPs *by Bauhinia racemosa* leaf extract.

TEM was used to analyze the particle size and shape. TEM images of the catalysts produced for this study are shown in Fig. 9. While the catalysts were variable in shape and size, most were spherical, with sizes ranging from 5 to 100 nm. In the presence of studies, the agglomeration of prepared manganese ferrite samples is magnetic interaction between the nanoparticles. The average particle size was found to be 15 nm; the length of the individual selected particles measured in images j viewer software is shown in Figs. 9, (a**,** b**,** c) and HR-TEM images analysis estimated particle size, which is in good agreement with the XRD result [28]. Fig. 9 (d) shows the selected area electron diffraction (SAED) pattern repressing sharp rings, which reveals the good crystalline of the Co_3O_4 NPs.

3.3. *Cyclic voltammetry studies*

Cyclic Voltammetry was first tested by the electrode system of three, where Ag was the reference and the counter-electrode was platinum. Fig.10a reveals the CV curve of Co_3O_4 NPs in a potential range from -1.7- to +1.7 V. From the CV curve, very clear and shrill redox peaks appeared, showing the nature of pseudo capacitance. Because redox reactions mainly rely on the insertion and dis-insertion of protons of the electrolyte at decreasing scan rates, the distribution of ions from the electrolyte knows how to come into nearly all the operational fleapits of the electrode. The shape of curves has diverted from an ultimate rectangular shape that indicates the pseudo-capacitive action of cobalt oxides [27-29]. The faradaic reactions can be explained by the below equations

$$Co_3O_4 + OH^- + H_2O \longleftrightarrow 3CoOOH + e^- \text{ ……..(2)}$$

$$CoOOH + OH^- \longleftrightarrow CoO_2 + H_2O + e^-. \text{ ……(3)}$$

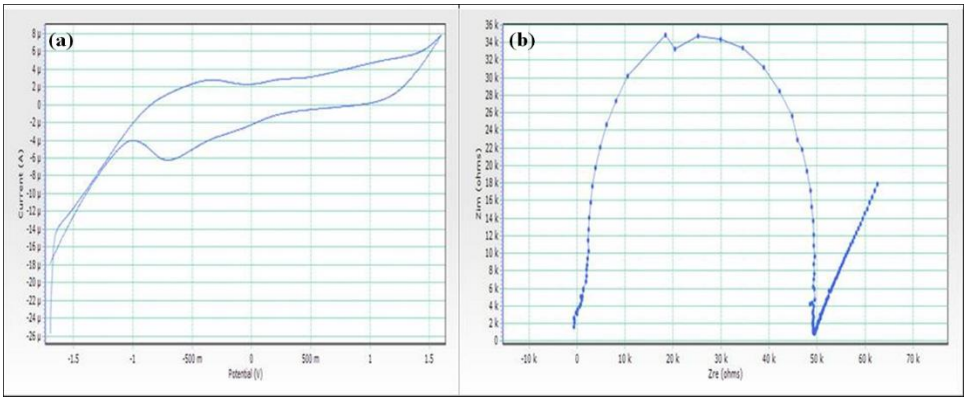

Fig.10. (a) CV image of Co_3O_4 NPs, (b) impedance spectrum of Co_3O_4 NPs.

This CV depicts the GCD behavior of the three-electrode cell of Co_3O_4 on various current densities. Its shape indicates the pseudo-capacitive action of Co_3O_4, which is also shown by cyclic voltammetry. For a range of current densities from 1 mA cm^{-2} to 10 mA cm^{-2}, SCs of Co_3O_4 varied from 698.4 F g^{-1} to 269.69 F g^{-1}. Fig. 10b demonstrates the Co_3O_4 electrode Electrochemical Impedance Spectroscopy. The ionic motion between the electrode and electrolyte surface was observed by EIS within the frequency range of 1 to 100 kHz through 5 mV of amplitude. The Co_3O_4 electrode charging transfer resistance (Rct) is very small, which indicates that effective electrochemical reaction sites are enough. Additionally, the Co_3O_4 electrode's diffusion resistance is lower, enabling the diffusion of ions in the redox reaction phase.

3.4. *Biological studies*

3.4.1. *Antioxidant*

Total antioxidant activity

The total antioxidant activities of samples were observed. About 3 mL of antioxidant reagent (0.6 M H_2SO_4, 28 mM Na_3PO_4, and 4 mM ammonium molybdate) were mixed to the test samples of Co_3O_4 NPs mediated by aqueous extract of *Bauhinia racemosa* (Thiruvachi) leaves with various concentrations (50, 100, 200, 250, 500) µg/mL. The test mixture to realize appropriate dispersion with phosphomolybdenum substance was incubated at 95 ^oC for 90 min in a water bath. The total antioxidant activity [30-31] of extracts and vitamin C standard drugs were measured and determined their absorbance at 695 nm using a spectrophotometer. The inhibition image has shown in Fig.11a, and the percentage of inhibition has shown in Table 1. The total antioxidant activities were calculated using the given formula.

$$TOA = [(A_t - A_c) / A_t] X\ 100.$$

Table. 1. Antioxidant, anti-diabetic, and anti-inflammatory activity of Co_3O_4 NPs by aqueous Bauhinia racemosa (Thiruvachi) leaves extract.

	Antioxidant activity		Anti-diabetic activity		Anti-inflammatory	
Concentration	% inhibition (λ_{max}nm)	% inhibition Standard (λ_{max}nm)	% inhibition (λ_{max}nm)	% inhibition Standard (λ_{max}nm)	% inhibition (λ_{max}nm)	% inhibition Standard (λ_{max}nm)
50	7.8947	31.3725	23.3846	29.8461	33.4164	22.6932
100	14.6341	50.7042	36.8205	46.4615	46.5087	36.7831
200	22.2222	83.9449	51.3846	61.3333	56.2344	46.6334
250	31.3725	92.8716	72.6153	76.5128	67.8304	58.7281
500	40.6779	97.1796	79.3846	85.2307	88.5286	79.1772

3.4.2. *Anti-diabetic activity*

α-Amylase inhibition technique method: Briefly, amylase (0.2 %) was incubated with and without samples (in 1.5 mL) and standard for 10 min at 25 °C. This experiment was performed in 0.2 M phosphate buffer (pH 6.9). After pre-incubation, the 1 % starch solution (0.5 mL) was added, and the Co_3O_4 NPs were incubated for 30 min at 25 °C. So as to stop the enzymatic reaction, DNSA reagent (0.5 mL) was added as the color reagent and then incubated in a boiling water bath for 90 min. Then cooling to room temperature, 0.5 mL of samples were diluted to 2.5 mL of distilled water, and the absorbance was unhurried at 540 nm using a UV-Visible spectrophotometer [32,33]. The measured absorbance was compared with that of the control experiment. The inhibition image is shown in Fig. 11b, and the percentage of inhibition has shown in Table 1. The % inhibition was calculated from the given formula.

$$\% \text{ of Inhibition} = 100 \times [Ac\text{-}At / Ac]$$

3.4.3. *Anti-inflammatory activity*

BSA denaturation technique: The Co_3O_4 NPs and standard diclofenac sodium were curtained for anti-inflammatory activity by inhibiting albumin denaturation modus operandi with minor modification [34-38]. The standard drug and compound were dissolved in a minimum quantity of dimethyl formamide (DMF) and diluted with phosphate buffer (0.2 M, PH 7.4). The final concentration of DMF in all solutions was less than 2.5 %. Test Solution (2.5 mL) containing different drug concentrations was mixed with 1 mL of 1 mM bovine serum albumin solution in phosphate buffer and incubated at 37 °C in an incubator for 10 min. Denaturation was induced by keeping the reaction mixture at 70 °C in a water bath for 10 min. After cooling, the turbidity was measured at 660 nm. The percentage of denaturation inhibition was calculated from the control where no drug was added. The inhibition image is shown in Fig. 11c, and the percentage of inhibition is shown in Table 1. The percentage inhibition of denaturation was calculated using the following formula.

% of Inhibition = 100 x[Ac-At /Ac]

At: Absorbance of test

Ac: Absorbance of control

The anti-diabetic activity of the samples was performed using α-amylase inhibition

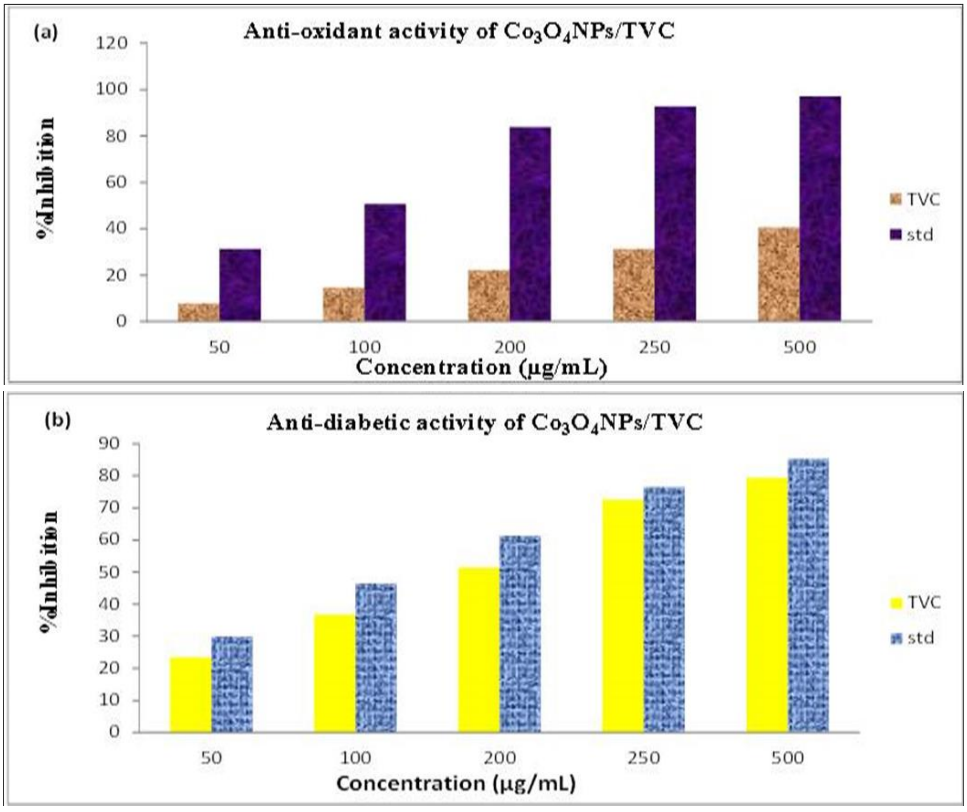

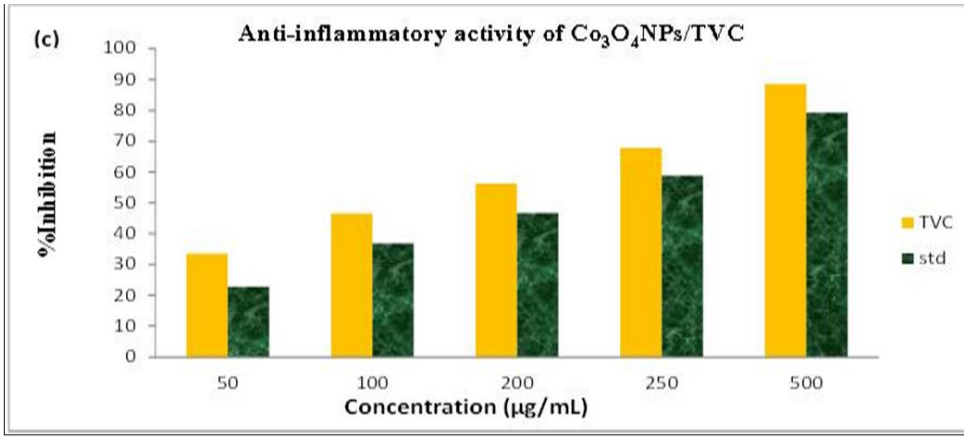

Fig. 11. (a) Antioxidant, (b) anti-diabetic, and (c) anti-inflammatory activity of Co_3O_4 NPs by aqueous extract *of Bauhinia racemosa (Thiruvachi) leaves.*

4. Conclusion

A green route was applied to synthesize Co_3O_4 NPs using *Bauhinia racemosa* (Thiruvachi) leaves extract. For the production of nanoparticles, this process is easy, ecologically benign, the most efficient, and less expensive. The formation of Co_3O_4 NPs was verified by UV and FTIR spectroscopy. Fluorescence effects were recorded by FL spectroscopy. The sample calcined at 350 °C was amorphous. The amorphous phase evolves into a crystalline phase as the calcination rises. The XRD also confirms the various geometries of synthesized Co_3O_4 NPs. Because of the increase in particle size, the band gap energy decreases with temperature. Electrochemical characterization of Co_3O_4 NPs was carried out using CV and EIS techniques. The Co_3O_4 NPs significantly showed antioxidant, anti-diabetic and anti-inflammatory activity. The outcome of the research confirms that the leaf phytochemicals of *Bauhinia racemosa* are responsible for forming Co_3O_4 NPs and prove to be a good antioxidant, anti-diabetic agent, and excellent anti-inflammatory agent.

Reference

1. Y. A. M. Esa and N. Sapawe, Mater. Today Proc. **31**, 386 (2020). https://doi.org/10.1016/J.MATPR.2020.07.184
2. A. Rana, K. Yadav, and S. Jagadevan, J. Clean. Prod. **272**, ID 122880 (2020). https://doi.org/10.1016/j.jclepro.2020.122880
3. A. Miri, M. Sarani, M. R. Bazaz, and M. Darroudi, Spectrochim. Acta Part A Mol. Biomol. Spectros. **141**, 287 (2015). https://doi.org/10.1016/j.saa.2015.01.024
4. S. Abinaya, H. P. Kavitha, M. Prakash, and A. Muthukrishnaraj, Sustain. Chem. Pharm. **19**, 100368 (2021). https://doi.org/10.1016/j.scp.2020.100368
5. A. K. Singh and J. K. Singh, Prog. Org. Coating **131**, 301 (2019). https://doi.org/10.1016/j.porgcoat.2019.02.025

6. M. Pahlavan, Noghabi, M. R. Parizadeh, M. Ghayour-Mobarhan, D. Taherzadeh, H. A. Hosseini, and M. Darroudi, J. Mol. Struct. **1146**, 499 (2017). https://doi.org/10.1016/j.molstruc.2017.05.145
7. K. P. Singh, A. K. Singh, and S. Gupta, Environ. Sci. Pollut. Res. **19**, 3914 (2012). https://doi.org/10.1007/s11356-012-1005-y
8. N. Sarwar, U. B. Humayoun, M. Kumar, S. F. A. Zaidi et al., J. Clean. Prod. **292**, ID 125974 (2021). https://doi.org/10.1016/j.jclepro.2021.125974
9. M. K. H. M. Nazri and N. Sapawe, Mater. Today Proc. **31**, A48 (2020). https://doi.org/10.1016/j.matpr.2020.10.968
10. A. K. Singh and K. P. Singh, Res. Chem. Intermed. **42**, 2247 (2016). https://doi.org/10.1007/s11164-015-2147-6
11. A. K. Singh and K. P. Singh, Appl. Water Sci. **8**, 226 (2018). https://doi.org/10.1007/s13201-018-0875-7
12. P. Maleki, F. Nemati, A. Gholoobi, A. Hashemzadeh, Z. Sabouri, and M. Darroudi, Inorg. Chem. Commun. **131**, ID 108762 (2021). https://doi.org/10.1016/j.inoche.2021.108762
13. D. C. Onwudiwe, M. P. Ravele, and E. E. Elemike, Nano-Struct. Nano-Objects. **23,** 100470 (2020). https://doi.org/10.1016/J.NANOSO.2020.100470
14. M. S. Samuel, E. Selvarajan, T. Mathimani, N. Santhanam, *et al*., J. Photochem. Photobiol. B Biol. **211,** ID 112011 (2020). https://doi.org/10.1016/j.jphotobiol.2020.112011
15. N. Akhlaghi, G. Najafpour-Darzi, and H. Younesi, Adv. Powder Technol. **31**, 3562 (2020). https://doi.org/10.1016/j.apt.2020.07.004
16. G. Asha, V. Rajeshwari, G. Stephen, S. Gurusamy *et al*., Mater. Today Proc. **48**, 486 (2022). https://doi.org/10.1016/j.matpr.2021.02.338
17. S. Dey and G. C. Dhal, Mater. Today Chem. **14**, ID 100198 (2019). https://doi.org/10.1016/J.MTCHEM.2019.100198
18. F. Thema., P. Beukes., A. Gurib-Fakim, and M. Maaza, J. Alloys Compd. **646**, 1043 (2015). http://dx.doi.org/10.1016/j.jallcom.2015.05.279
19. A. B Birusanti, U. Mallavarapu, D. Nayakanti, C. S Espenti, and S. Mala. IET Nanobiotech **13**, 71 (2019). https://doi.org/10.1049/iet-nbt.2018.5117
20. B. Gawade and M. Farooqui, Asian J. Pharma. Clin. Res. **11,** 190 (2018). http://dx.doi.org/10.22159/ajpcr.2018.v11i6.24038
21. D. Demandol and J. Davoust, J. Micro. **185**, 21 (1997). https://doi.org/10.1046/j.1365-2818.1997.1470704.x
22. F. C. Okwunodulu, H. O. C. Okorie, and F. C. Okorie, Chem. Sci. Int. J. **27,** 1 (2019). https://doi.org/10.9734/CSJI/2019/v27i130106
23. D. Malathy and M. Revathi, Res. J. Pharm. Tech. **14,** 1530 (2021). https://doi.org/10.5958/0974-360X.2021.00271.7
24. S. Haq, F. Abbasi, M. B. Ali, A. Hedfi, *et al*., Mater. Res. Express. **8,** ID 075009 (2021). https://doi.org/10.1088/2053-1591/ac1187
25. S. Rajeshkumar, J. Genet. Eng. Biotechnol. **14,** 195 (2016). https://doi.org/10.1088/2053-1591/ac1187
26. R. Mogomotsi, S. S. Akinola, E. E. Emeka, and O. E. Fayemi, Mater. Res. Express **7**, ID 055001 (2020). https://doi.org/10.1088/2053-1591/ab8ba1
27. N. Maouche and B. Nessark, Int. J. Electrochem. **5,** ID 670513 (2011). https://doi.org/10.4061/2011/670513
28. M. H. Priyadarsini, M. C. Adhikary, P. Jena, and R. M. Pujahari, J. Sci. Res. **15**, 43 (2023). http://dx.doi.org/10.3329/jsr.v15i1.59397
29. K. Anandalakshmi and P. Venkatachalam, J. Venugobal, J. Sci. Res. **15**, 1 (2023). http://dx.doi.org/10.3329/jsr.v15i1.56206
30. T. Santhoshkumar, A. A. Rahuman, C. Jayaseelan, G. Rajakumar *et al*., Asian Pac. J. Trop. Med. **7,** 968 (2014). https://doi.org/10.1016/S1995-7645(14)60171-1
31. J. Vyas and S. Rana, Int. J. Phytomed. **9**, 634 (2017). https://doi.org/10.5138/09750185.2185

32. N. Bala, S. Saha, M. Chakraborty, M. Maiti *et al*., RSC Adv. **5**, 4993 (2015). https://doi.org/10.1039/C4RA12784F
33. H. Hou, B. Mahdavi, S.Paydarfard, M. M. Zangeneh *et al*., Sci. Rep. **10,** 12195 (2020). https://doi.org/10.1038/s41598-020-68951-x
34. P. Singh, S. Ahn, J. Kang, S. Veronika et al., Artif. Cells Nanomed. Biotechnol. **46**, 2022 (2018). https://doi.org/10.1080/21691401.2017.1408117
35. N. Muniyappan, M. Pandeeswaran, and A. Amalraj, Environ. Chem. Ecotoxicol. **3**, 117 (2021). https://doi.org/10.1016/j.enceco.2021.01.002
36. R. E. Varghese, D. Ragavan, S. Sivaraj, D. Gayathri, and G. Kannayiram, Asia J. Pharm. Clin. Res. **10**, 370 (2017). https://doi.org/10.22159/ajpcr.2017.v10i11.19904
37. P. B. E. Kedi, B. N. Etah, V. Deli, A. P. Gbambie *et al*., IJGHC, Sec. B **9**, 345 (2020). https://doi.org/10.24214/IJGHC/HC/9/3/34560
38. G. Vanitha, R. Manikandan, A. Prakasam, M. D. Navinkumar, K. Sathiyamoorthi, B. Dhinakaran, IJGHC **12,** 30 (2023). https://doi.org/10.24214/IJGHC/HC/12/1/03041